fire

MDPI

Article

Thermal Decomposition Mechanism of PF_5 and POF_3 with Carbonate-Based Electrolytes During Lithium-Ion Batteries' Thermal Runaway

Yao Tian [1,2,3,*], Xiaotiao Zhan [1], Yuxin Zhang [2], Zhen Qiao [1,2], Yuxiang Lu [1], Qing Xia [1], Jian Lu [3,4], Xia Zhang [1,*] and Zhaoyang Chen [3,*]

[1] Safety and Quality Technology Research Center, China Waterborne Transport Research Institute, Beijing 100088, China
[2] School of Emergency Management and Safety Engineering, China University of Mining and Technology, Beijing 100083, China
[3] Institute of Materials Research, Tsinghua Shenzhen International Graduate School, Tsinghua University, Shenzhen 518055, China; lujian@szpu.edu.cn
[4] Advanced Energy Storage Technology Research Center, Shenzhen Polytechnic University, Shenzhen 518055, China
* Correspondence: tianyao@wti.ac.cn (Y.T.); zhangxia@wti.ac.cn (X.Z.); chency20@tsinghua.org.cn (Z.C.)

Abstract

Against the background of the accelerating global transition towards a low-carbon energy system, the lithium-ion battery (LIB) industry has witnessed a rapid development. Concurrently, fire accidents in LIB application scenarios have occurred frequently, with safety issues becoming increasingly prominent. Thermal runaway of LIBs is the direct cause of such fires. During the thermal runaway process of LIBs, lithium salts in the electrolyte undergo thermal decomposition reactions with carbonate-based electrolytes, releasing a large amount of heat and fire gases. Among them, the thermal decomposition reactions of $LiPF_6$ with electrolytes are coupled and superimposed, exhibiting a significant synergistic effect. This paper employs quantum chemical calculation methods to investigate the thermal decomposition reaction mechanisms between PF_5 and POF_3, which generated from the thermal decomposition of $LiPF_6$ and carbonate-based electrolytes (EC, DMC, and DEC) during the thermal runaway process of LIBs; and presents detailed chemical reaction mechanism models. The P atoms in PF_5 or POF_3 combine with the O atoms of the ether oxygen groups in carbonates, while the F atoms combine with the C atoms adjacent to the ether oxygen groups. This promotes the ring-opening or chain scission of carbonate molecules, reduces the energy required for the reaction, and accelerates the thermal decomposition reaction and the generation of fire gases. Modification of EC, DMC, and DEC through fluorination can effectively inhibit the catalytic effect of PF_5 and POF_3 and improve the oxidation resistance and thermal stability of the electrolytes.

Keywords: lithium-ion battery; PF_5; POF_3; electrolyte; thermal decomposition reaction; quantum chemical calculation

check for updates

Academic Editors: Jian Wang, Jingwen Weng, Que Huang and Ao Li

Received: 18 August 2025
Revised: 7 September 2025
Accepted: 16 September 2025
Published: 19 September 2025

Citation: Tian, Y.; Zhan, X.; Zhang, Y.; Qiao, Z.; Lu, Y.; Xia, Q.; Lu, J.; Zhang, X.; Chen, Z. Thermal Decomposition Mechanism of PF_5 and POF_3 with Carbonate-Based Electrolytes During Lithium-Ion Batteries' Thermal Runaway. *Fire* **2025**, *8*, 370. https://doi.org/10.3390/fire8090370

Copyright: © 2025 by the authors. Licensee MDPI, Basel, Switzerland. This article is an open access article distributed under the terms and conditions of the Creative Commons Attribution (CC BY) license (https://creativecommons.org/licenses/by/4.0/).

1. Introduction

Under the overarching context of the globally accelerated transition toward a low-carbon energy system, lithium-ion batteries (LIBs) have emerged as the core technological enabler in the energy storage and conversion sector, primarily attributed to their inherent advantages of high energy density, long cycle life, and low self-discharge rate. These

attributes have propelled their widespread adoption across critical domains, including electric vehicles, large-scale energy storage systems (ESSs), and portable electronic devices, thereby solidifying their pivotal role in modern energy infrastructure. Notably, the global LIB market demonstrated robust growth in 2024, with total shipments reaching 1545.1 GWh, representing a year-on-year increase of 28.5% [1].

Meanwhile, behind the vigorous development of the LIB industry, safety issues concerning LIBs, particularly fire hazards, have become increasingly prominent. In recent years, LIB fires have shown a frequent occurrence globally, with multiple severe fire accidents attracting widespread attention. In May 2024, a fire broke out at the Gateway Energy Storage Station in California, USA, during which a large amount of toxic gases was released. The fire reignited twice and burned for six days, forcing the evacuation of nearby residents. In June 2024, a fire occurred at the Aricell lithium battery factory in Hwaseong City, Gyeonggi-do, South Korea, resulting in 23 deaths. In June 2025, the roll-on/roll-off cargo ship "Morning Midas" caught fire in the waters off Alaska, USA, destroying 800 electric vehicles, hybrid vehicles, and over 2200 other fuel-powered vehicles on board, eventually leading to the sinking of the ship. In the first half of 2025 alone, there have been at least 15 fire safety incidents in global civil aviation caused by LIB power banks carried by passengers, a significant increase compared with the same period in 2024. The fire risks in application scenarios of LIBs such as LIB energy storage stations, electric vehicles, electric bicycles, and electronic products cannot be ignored either, posing severe challenges to public life and property safety as well as the sustainable development of the industry.

LIBs fires are caused by thermal runaway. Thermal runaway of LIBs are a serious chain exothermic reaction process triggered by the coupling of multi-scale and multi-physical fields inside them, and their mechanisms involve the synergistic effect of electrode materials, electrolytes, and interface reactions [2,3]. When LIBs are subjected to mechanical abuse (such as crushing and piercing), electrical abuse (overcharging and short circuit), or thermal abuse (high ambient temperature), they first trigger the thermal self-exothermic decomposition reactions of the solid electrolyte interphase (SEI) film on the surface of their negative electrode, releasing gases such as CO_2, C_2H_4, CO, and H_2 along with some heat. As the temperature rises to 120–200 °C, the lithium intercalated in the negative electrode reacts with organic solvents in the electrolyte (such as ethylene carbonate (EC), dimethyl carbonate (DMC), and diethyl carbonate (DEC)), generating Li_2CO_3 and flammable gases like, CO_2, CO, and H_2 and releasing a large amount of heat. Meanwhile, lithium salts in the electrolyte (such as $LiPF_6$) undergo thermal decomposition reactions, and the products further combine with the electrolyte and promote oxidative decomposition reactions, releasing toxic gases such as HF, PF_5, and POF_3 and heat [4–7]. As the temperature continues to rise, the separator inside the battery melts, leading to internal short circuits. When the temperature further increases to 200–300 °C, positive electrode materials (such as Li_2CoO_2, $LiFePO_4$, and $LiNi_xCo_yMn_zO_3$) decompose, releasing O_2 which reacts with organic solvents in the electrolyte and releasing a large amount of heat. At this stage, the electrolyte continues to decompose to produce toxic gases such as HF and CO, which form a flammable gas mixture with the products of electrode reactions and deflagrate at high temperatures [8,9].

The above reactions form a positive feedback cycle of "exothermic reaction, temperature rise, reaction intensification", eventually causing rupturing of the battery casing, electrolyte volatilization, and flame jetting while releasing a large amount of fire gases. During the thermal runaway and combustion process of LIBs, most of the fire gases are derived from the thermal decomposition and oxidation reactions of the electrolyte. Meanwhile, the reaction temperature has a significant impact on the modes of thermal decomposition and

oxidation reactions, as well as the types and quantities of products generated. In addition, during the thermal runaway and combustion process of LIBs, the rapid evaporation, oxidation, and thermal decomposition of the electrolyte lead to a sharp increase in the internal pressure of the battery, resulting in the destruction of the internal pole piece structure and causing changes in the internal flow field of the battery. The rise in the internal pressure of the battery, along with the thermal decomposition and oxidation reactions of the electrolyte and the migration of fire gases, further affect the combustion reaction mode and intensify the thermal runaway process [10–12].

$LiPF_6$ is the most widely used lithium salt in LIB electrolytes. Its core function is to dissociate into Li^+ and PF_6^- in carbonate-based solvents, providing a conductive carrier for the migration of lithium ions between the positive and negative electrodes, forming a high ionic conductivity system, and ensuring the battery's charge–discharge efficiency. Meanwhile, $LiPF_6$ participates in the formation of the SEI film on the negative electrode; at high concentrations, it can promote the generation of inorganic components such as LiF and can optimize interface stability, and it exhibits good compatibility with aluminum current collectors, being suitable for high-voltage cathode materials. The thermal instability of $LiPF_6$ is one of the key factors inducing thermal runaway in LIBs [13–16]. $LiPF_6$ begins to decompose into LiF and PF_5 at approximately 107 °C. As a strong Lewis acid, PF_5 catalyzes the decomposition of solvents, releasing a large amount of heat. Furthermore, PF_5 reacts with trace amounts of water to generate HF and POF_3. HF damages the SEI film and corrodes electrodes, exacerbating side reactions [17–20]. PF_5 and POF_3 continuously promote solvent decomposition through autocatalytic chain reactions and synergize with thermal decomposition of EC, DMC, and DEC, leading to a sudden rise in the temperature of the battery and ultimately triggering combustion or explosion. The massive generation of fire gases such as HF, CO, CO_2, and C_2H_4 during this process further intensifies the increase in internal pressure of the battery and the spread of thermal runaway [21–24].

Relevant studies have shown that PF_5 and POF_3, the thermal decomposition products of $LiPF_6$, can catalyze the chain oxidation reactions of organic solvents, reducing the critical temperature for thermal runaway by 10–30 °C. Many scholars have conducted experimental studies on the reaction mechanisms between $LiPF_6$ and electrolyte components such as EC, DMC, DEC, and EMC and proposed preliminary thermal decomposition reaction mechanisms [25–27]. In the field of LIB fire research, the kinetic studies on the thermal decomposition and oxidation reactions of electrolytes are still in their infancy. The existing experimental data and reaction models are relatively simplistic, lacking detailed chemical reaction mechanism models, intermediate products, and reaction kinetic parameters. The analysis of the synergistic decomposition effects in mixed solvent systems and the dynamic evolution of free radical chain reactions is insufficient; most models are simplified to main reaction pathways, making it difficult to quantify the energy changes during thermal runaway and the generation rates of fire products. Consequently, combustion kinetic analysis and fire numerical simulations for LIBs still exhibit significant inaccuracies, which constrain the design and development of high-safety LIBs.

In recent years, there have been many research studies on the fire numerical simulation of LIBs using CFD software. Fire numerical models have been developed to build up synthetic data from fire experiments at different scales of LIBs such as cell, pack, vehicle, and energy storage systems [28–30]. They can provide fast predictions of the consequences of fire development. A key challenge for numerical modeling is the representation of the fire performance of LIBs properties. At present, the numerical simulation process for LIB fires usually involves directly inputting the heat release law and fire gas release law of a specific type of battery measured in the laboratory into the CFD program for calculation. This simulation process ignores the influence of different sizes and different combustion

conditions on fire behavior, and the simulation results usually have a certain deviation from the actual situation. This is because research on the combustion and kinetic mechanism of LIBs is still in its infancy, and an accurate and complete detailed chemical reaction mechanism model for thermal decomposition and oxidation has not yet been established.

The kinetic simulation of electrolyte combustion reactions forms the foundation for research on LIBs fires, relying heavily on the accurate description of chemical reaction mechanisms and precise prediction of thermodynamic and kinetic data of reactions. In recent years, with the advancement of quantum chemical methods and computational capabilities, theoretical calculation approaches have been increasingly widely applied to predict and analyze chemical reaction mechanisms under combustion conditions [31]. In our previous research studies, we employed quantum chemical calculation methods to elaborate in detail on the thermal decomposition reaction mechanisms, oxidation reaction mechanisms, and fire gas generation patterns of main electrolyte components (EC, DMC, and DEC), as well as the catalytic effect of Li^+ on the thermal decomposition reactions of electrolytes during the thermal runaway process of LIBs [21,32].

In this paper, we employ quantum chemical calculation methods to further analyze the reaction mechanisms between PF_5 and POF_3 (thermal decomposition products of $LiPF_6$) and the main electrolyte components (EC, DMC, and DEC) in LIB electrolyte systems. Additionally, we explore the theoretical basis for improving the oxidation resistance and flame retardancy of LIBs by using fluorinated electrolytes. By clarifying these mechanisms, which represent the core contributions and innovations of this study, we aim to establish a solid theoretical foundation for the combustion reaction mechanisms of electrolytes and provide theoretical support for subsequent in-depth research on LIB fire mechanisms, as well as the construction of numerical models to enhance battery fire resistance.

2. Materials and Methods

2.1. Computational Contents

During the thermal runaway process of LIBs, the electrolyte undergoes thermal decomposition and oxidation reactions, generating a large amount of fire gases. Significant differences exist in heat release characteristics and fire gas emission patterns during the thermal runaway process of LIBs with different states of charge (SOCs). For thermal runaway caused by puncture or short circuit, the battery temperature rises rapidly, with a heating rate of up to 100 °C/min, and the maximum temperature may exceed 600 °C. On the other hand, the heating rate is relatively slow for thermal runaway triggered by battery aging or heat accumulation. Therefore, there may be two forms of thermal decomposition and oxidation reactions of the electrolyte during the thermal runaway process of LIBs: The first one occurs when the battery heating rate is fast and the battery temperature is high, where the electrolyte heats up rapidly and directly undergoes thermal decomposition and oxidation reactions in a liquid environment. The second one takes place when the battery heating rate is slow and the battery temperature is low, in which case the electrolyte first evaporates into a gaseous state and then further undergoes thermal decomposition or oxidation reactions in a gaseous environment. Hence, this paper investigates the thermal decomposition reaction mechanisms of the electrolyte in both the electrolyte environment and the air environment, aiming at the above two different combustion forms of the electrolyte.

In this paper, a composite electrolyte composed of EC, DMC, and DEC at a volume ratio of 1:1:1 is selected as the research object, with $LiPF_6$ being used as the lithium salt electrolyte at a concentration of 1 mol/L. In this paper, we analyze the thermal decomposition reaction mechanisms of PF_5 and POF_3 with EC, DMC, and DEC molecules in both an electrolyte environment and air environment. All calculations in this paper are performed by using

the software of Gaussian 16 [33] and Gauss View 6.0 [34]. The molecular model of the electrolyte solvent is shown in Figure 1.

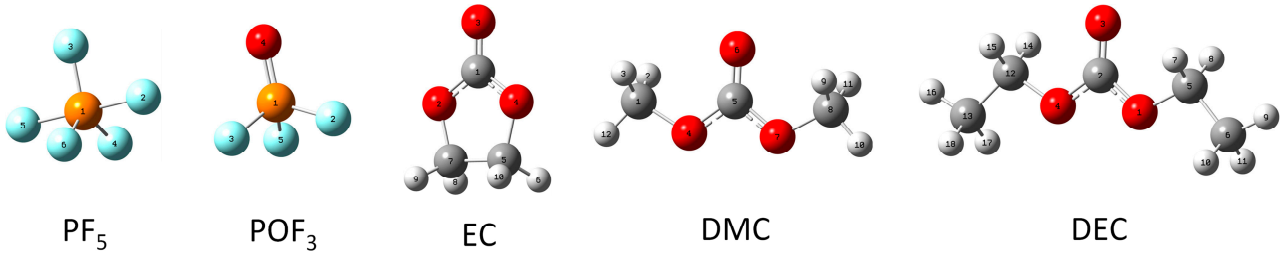

Figure 1. Configurations of main constituents of the electrolyte. Note: Cyan represents fluorine (F), orange represents phosphorus (P), gray represents carbon (C), red represents oxygen (O), and white represents hydrogen (H).

2.2. Computational Methods

2.2.1. Methods of Electrolyte in Its Liquid Environment

In this paper, we investigate the thermal decomposition reaction mechanisms of PF_5 and POF_3 with EC, DMC, and DEC in an electrolyte environment, which is simulated by using an implicit solvent model. And the implicit solvent model describes solvent properties from a macroscopic perspective, ignoring the microscopic state of solvent molecules and treating the solvent as a continuous and uniformly distributed medium. The advantage of the implicit solvent model lies in its ability to accurately represent the average effect of the solvent while significantly reducing the computational load. Therefore, it is widely used in the fields of quantum chemistry and molecular simulation.

In this paper, we use quantum chemical simulations to perform the density functional theory (DFT) method combined with the solvation model based on density (SMD). And the dielectric constant of the electrolyte is the sum of the dielectric constants of its main components (EC, DMC, and DEC) multiplied by their respective volume ratios. The dielectric constants of the main components in the electrolyte are presented in Table 1.

Table 1. Description of electrolyte environment parameters.

No.	Constituents	Dielectric constants
1	EC	87.780
2	DMC	3.107
3	DEC	2.805
4	Electrolyte	31.897

For the calculations of the reactions in the electrolyte environment, we perform geometric optimization of the molecules and functional groups by using the B3LYP density functional and 6-311++G (d,p) basis set, with dispersion force correction and thermodynamic correction being taken into consideration. And then, the M06-2X/6-31G (d) basis set is adopted to conduct high-precision electronic energy calculation on each geometrically optimized molecule and group, followed by Gibbs free energy calculation. The formula for calculating the Gibbs free energy of each molecule and group is as follows:

$$\Delta G = E + G_{(\mathrm{corr})} \tag{1}$$

$$\Delta G_{\mathrm{dec.(AB)}} = \Delta G_{\mathrm{A}} + \Delta G_{\mathrm{B}} - \Delta G_{\mathrm{AB}} \tag{2}$$

ΔG represents the Gibbs free energy in kJ/mol; E represents electronic energy at the M06-2X/6-31G (d) level in kJ/mol; $G_{(\mathrm{corr})}$ represents the Gibbs free energy correction factor

at the B3LYP/6-311++G (d,p) level in kJ/mol; $\Delta G_{dec.(AB)}$, represents the reaction Gibbs free energy of the process when molecule or functional group AB decomposes into molecule or functional groups A and B, in kJ/mol; and ΔG_{AB}, ΔG_{A}, and ΔG_{B} represent the Gibbs free energy of molecule or functional group AB, A, and B, respectively, in kJ/mol.

2.2.2. Methods of Electrolyte in Air Environment

For the calculations in the air environment, we perform geometric optimization of the B3LYP density functional and 6-311++G (d,p) basis set, with dispersion force correction and thermodynamic correction being taken into consideration. And then, the M06-2X/def2tzvp basis set is adopted to conduct high-precision electronic energy calculation on each geometrically optimized molecule and group, followed by Gibbs free energy calculation.

2.3. Transition State Search and Intrinsic Reaction Coordinate Pathway Analysis

In this paper, the TS Berny method is used to search for transition state (TS) substances in the reaction process; then, the intrinsic reaction coordinate (IRC) method is employed to verify the reaction paths of transition state substances so as to ensure that the transition state substances in the reaction process correspond to the reactants and products. And the TS searches are performed by using the same functionals and basis sets as those of the geometric optimizations mentioned above.

3. Results and Discussion

The medium environment in which LIB electrolyte molecules reside exerts a considerable impact on their oxidative property, reductive property, and thermal stability [21,35]. In the air environment, the electrolyte evaporates into a gaseous state, leading to a significant increase in intermolecular distances, and the interactions between solvent molecules become almost negligible. Compared with the air environment, the electrostatic intermolecular interactions within the electrolyte are stronger, and the solvent effect is prominent. The solvent effect refers to the phenomenon in liquid phase reactions where the physical and chemical properties of the solvent affect the reaction equilibrium and reaction rate, whose essence lies in the fact that solvent molecules alter the electrostatic interactions between groups. In the solvent environment, some thermal decomposition reaction pathways and their reaction energies may undergo changes. Therefore, in this paper, the reaction mechanisms of EC, DMC, and DEC with PF_5 and POF_3 in both the electrolyte environment and the air environment are analyzed, respectively.

In the electrolyte, $LiPF_6$ undergoes decomposition reactions during the charge–discharge or thermal runaway processes of LIBs, generating substances such as PF_5 and POF_3. The thermal decomposition reactions of $LiPF_6$ upon combination with H_2O are the key factors inducing LIBs' aging and thermal runaway. In our previous work, we have analyzed the reaction pathways and mechanism of $LiPF_6$ with H_2O in detail, and they are shown in the Supplementary Information of this paper, Figure S1a [21]. Similarly, EC and DMC can also undergo analogous reactions, and these reaction mechanisms are shown in Figure S1b,c.

Both PF_5 and POF_3 exhibit strong oxidizing properties. The PF_5 molecule adopts a trigonal bipyramidal structure, where the central P atom is surrounded by F atoms. Given the extremely high electron-withdrawing ability of F atoms, they strongly attract the electron cloud of the central P atom through an inductive effect, leading to a significant reduction in the electron cloud density of the P atom. This confers PF_5 a stronger ability to gain electrons, i.e., a stronger oxidizing property. The POF_3 molecule, on the other hand, has a tetrahedral structure with stable P=O double bonds. Compared with PF_5, the electron cloud density of POF_3's central P atom is significantly higher, resulting in a

relatively weaker oxidizing property. (The HOMO and LUMO of PF_5 and POF_3 are shown in Figure S2.)

3.1. Reactions of EC with PF_5 and POF_3

As one of the most core components in an LIB electrolyte, EC plays crucial roles such as dissolving lithium salts, facilitating ion conduction, and stabilizing electrode interfaces in the electrolyte. The dielectric constant of EC is much higher than that of other carbonate solvents such as DMC and DEC. And its high dielectric constant enables EC to efficiently dissolve ionic lithium salts and promote the dissociation of $LiPF_6$ into freely mobile ions of Li^+ and PF_6^-, which provides a high ion concentration in the electrolyte. The oxygen atoms (carbonyl oxygen and cyclic ether oxygen) in EC molecules can form coordinate bonds with Li^+, PF_5, and POF_3, and its strong coordination ability allows it to occupy a core position in the solvation sheath.

3.1.1. Reactions of EC with PF_5

Figure 2a shows the thermal decomposition reaction pathway of EC combining with PF_5 in the electrolyte environment. The symbol of TS in the figure represents the transition state species. Firstly, absorbing 185.37 kJ/mol of heat, the cyclic ether oxygen atom in the EC molecule and its adjacent methylene carbon atom combine with the phosphorus atom and fluorine atom in the PF_5 molecule, respectively. Meanwhile, the PF_5 molecule promotes a stretching of the C-O bond in the cyclic structure of the EC molecule to transform into TS1, which is a transition state. Subsequently, the cyclic structure of the EC molecule is broken at the C-O bond, where it combines with PF_5, and the P-F single bond where the F atom linking EC in the PF_5 molecule cleaves, generating a chain group $FCH_2CH_2OCOOPF_4$ and releasing 90.52 kJ/mol of energy. Then, the group of $FCH_2CH_2OCOOPF_4$ could undergo further thermal decomposition reactions divided into two concurrent pathways:

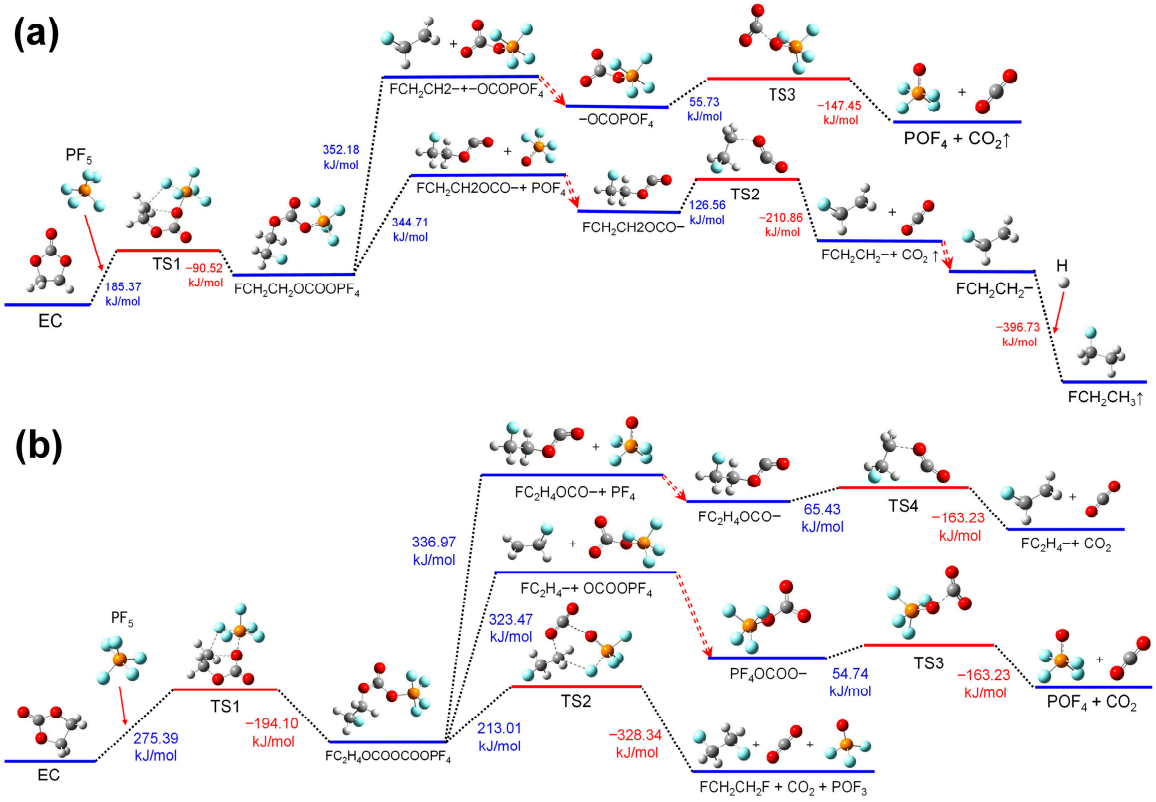

Figure 2. Reaction pathway of EC with PF_5. Note: (**a**) Reactions in the electrolyte environment; (**b**) reactions in the air environment.

(1) In the first pathway, absorbing 344.71 kJ/mol of heat, for the group of FCH_2CH_2OCOO PF_4, the C-O bond linking POF_4 cleaves and generates groups of POF_4 and FCH_2CH_2OCO-. Herein, absorbing 126.56 kJ/mol of heat, the group of FCH_2CH_2OCO- transforms into TS2, with the C-O bond stretching at the C atom of FCH_2CH_2-. And then, TS2 breaks into CO_2 and FCH_2CH_2-, releasing 210.86 kJ/mol of energy. The FCH_2CH_2- combines with a free H atom in the electrolyte to form a FCH_2CH_3 molecule.

(2) In the second pathway, absorbing 352.18 kJ/mol of heat, for the group of $FCH_2CH_2OCOOPF_4$, the C-O bond linking the group of FCH_2CH_2- cleaves and generates groups of FCH_2CH_2- and PF_4OCOO-. Then the group of PF_4OCOO- transforms into TS3, with the C-O bond stretching at the C atom being connected to POF_4, absorbing 55.73 kJ/mol of heat. And then TS3 breaks into POF4 and CO2, releasing 147.45 kJ/mol of energy.

Figure 2b shows the thermal decomposition reaction pathway of EC combining with PF_5 in the air environment. And these reactions are more complex than those in the electrolyte environment. Consistent with the reactions in the electrolyte environment, one F atom and the P atom in the PF_5 molecule combine with the cyclic ether O atom and its adjacent methylene's C atom in the EC molecule, respectively. Absorbing heat, the group transform into a state species of TS1. And then, TS1 undergoes ring-opening to generate a chain group of $FCH_2CH_2OCOOPF_4$ with an energy release.

In the air environment, there are three reaction pathways for $FCH_2CH_2OCOOPF_4$. Among them, the first two reaction pathways are the same as those in the electrolyte environment: the $FCH_2CH_2OCOOPF_4$ group undergoes bond cleavage at the C-O bond linking groups of FCH_2CH_2- and the PF_4O-, respectively. However, due to the disappearance of the solvation effect in the electrolyte environment, the reaction energy has changed.

In the third pathway, the group of $FCH_2CH_2OCOOPF_4$ absorbs heat and undergoes a reorganization reaction. The C-O bond linking the group of FCH_2CH_2- and the C-O bond linking the group of POF_4- stretch simultaneously. Meanwhile, a F atom in the group of POF_4- will combine with the -CH_2- of FCH_2CH_2- and the P-F bond linking this F atom stretch together. After this reorganization process, the group of $FCH_2CH_2OCOOPF_4$ transforms into TS2. Then, the TS2 decomposes into FCH_2CH_2F, CO_2, and POF_3, releasing energy.

In summary, the PF_5 molecule combines with the EC molecule, promoting its ring-opening and thermal decomposition reactions. This promoting effect is particularly significant in the electrolyte environment. The minimum energy required for the ring-opening reactions of EC is 290.89 kJ/mol [21,32], while after combining with PF_5, the ring-opening energy of EC decreases to 185.37 kJ/mol, representing a reduction of 36.27%. Therefore, PF_5 can accelerate the decomposition of the electrolyte during the thermal runaway process.

3.1.2. Reactions of EC with POF_3

Figure 3 shows the thermal decomposition reaction pathway of EC combining with POF_3. The reaction mechanisms of EC with POF_3 in electrolyte and air environments are similar to those of EC with PF_5. Due to the fact that the oxidizability of POF_3 is weaker than that of PF_5, the heat absorbed during the ring-opening reactions after POF_3 combines with EC is higher than that after PF_5 combines with EC, whether in the electrolyte environment or the air environment. The energy consumed during the further thermal decomposition reactions of the chain group of $FCH_2CH_2OCOOPOF_2$ generated after ring-opening is significantly higher than that of the $FCH_2CH_2OCOOPF_4$ group formed after PF_5 promotes the ring-opening of EC. Thus, POF_3 exhibits a weaker catalytic effect on promoting the thermal decomposition reactions of EC than that of PF_5.

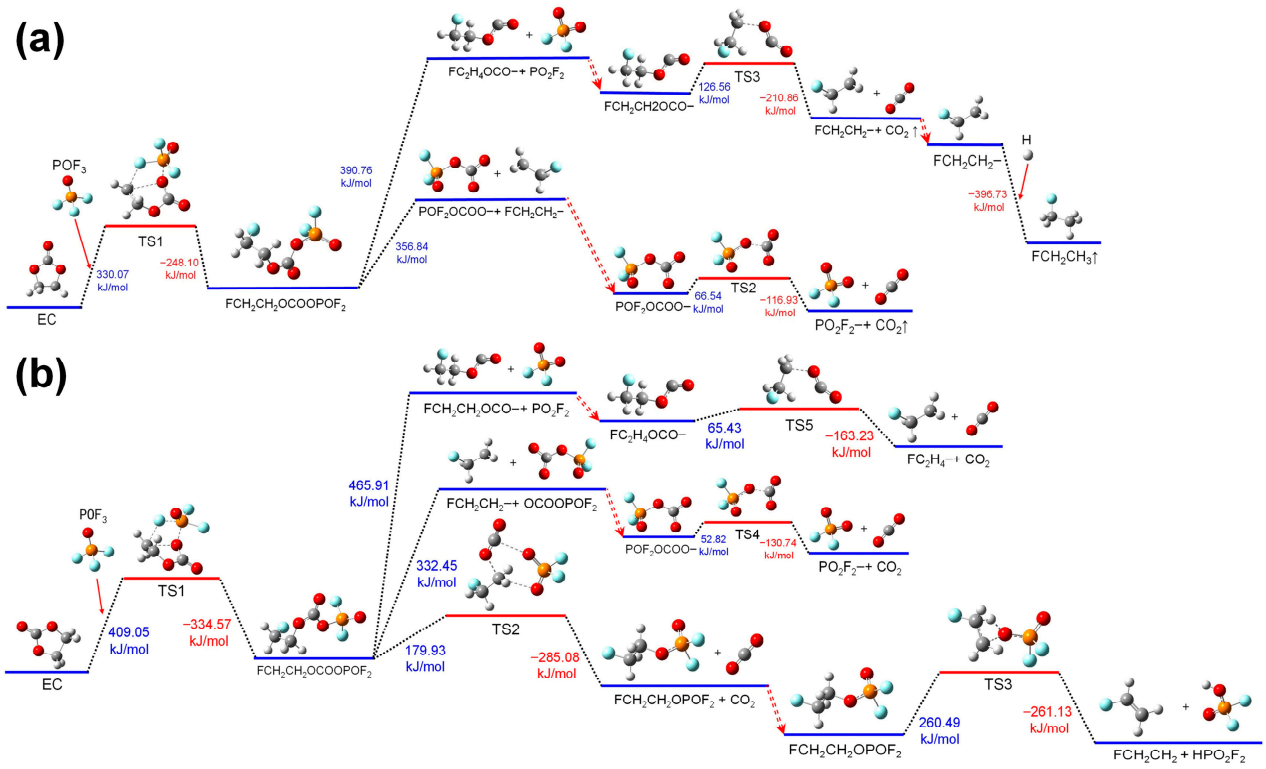

Figure 3. Reaction pathway of EC with POF_3. Note: (**a**) Reactions in the electrolyte environment; (**b**) reactions in the air environment.

In the air environment, in the third reaction pathway of the thermal decomposition process that occurs after EC combines with POF_3, there are certain differences between the reorganization process of the $FCH_2CH_2OCOOPOF_2$ group compared with that of the $FCH_2CH_2OCOOPF_4$ group. After absorbing heat, for the group of $FCH_2CH_2OCOOPOF_2$, the C-O bond linking FCH_2CH_2- and the C-O bond connecting with POF_2- stretch simultaneously, and the P=O bond in the POF_2- group stretches as well. Meanwhile, the O atom of POF_2- combines with the -CH_2- group at the end of the FCH_2CH_2- group to form the transition state substance of TS2. Then, the TS2 further decomposes into $FCH_2CH_2OPOF_2$ and CO_2. In this process, the FCH_2CH_2- group and the PO_2F_2- group undergo reorganization to form the group of $FCH_2CH_2OPOF_2$. Absorbing heat, for the group of $FCH_2CH_2OPOF_2$, the H atom on the FCH_2- group migrates to the O atom on the PO_2F_2 group. Meanwhile, with the C-O bond linking the FCH_2CH_2- group stretching, the $FCH_2CH_2OPOF_2$ transforms into TS3. Then, the TS3 further decomposes into $FCHCH_2$ and HPO_2F_2, releasing energy.

3.2. Reactions of DMC with PF_5 and POF_3

DMC ranks among the most critical solvents in LIB electrolytes. As a representative of linear carbonate solvents, DMC exhibits prominent features including low viscosity, low melting point, and excellent electrochemical stability. These intrinsic properties enable it to broaden the thermal stability window of the electrolyte, optimize the low-temperature performance of batteries, reduce electrolyte viscosity, mitigate the migration resistance of Li^+ ions, and thereby enhance the charge–discharge efficiency as well as rate capability.

3.2.1. Reactions of DMC with PF_5

Figure 4a shows the thermal decomposition reaction pathway of DMC combining with PF_5 in the electrolyte environment. Firstly, the O atom in the CH_3O- group of the DMC molecule binds to the P atom in PF_5, while the C atom of the same CH_3O- binds to the F

atom in the former PF_5. Absorbing energy, the C-O bond in the CH_3O- group and the P-F bond in PF_5 stretch, thereby forming the transition state substance TS1. Subsequently, the TS1 decomposes into CH_3F and $CH3OCOOPF_4$. Then, the group of $CH3OCOOPF_4$ could undergo further thermal decomposition reactions divided into two concurrent pathways:

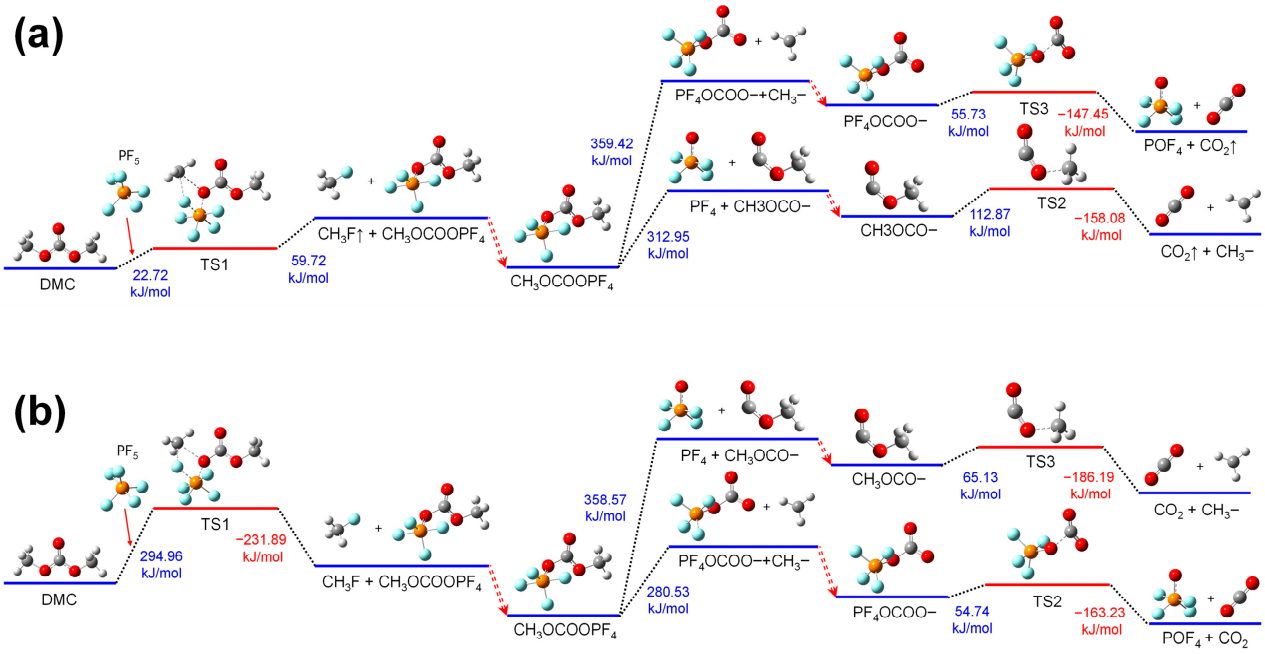

Figure 4. Reaction pathway of DMC with PF_5. Note: (**a**) Reactions in the electrolyte environment; (**b**) reactions in the air environment.

(1) In the first pathway, absorbing heat, the group of $CH_3OCOOPF_4$ breaks at the C-O bond linking POF_4 and CH_3OCO-. And then upon a further heat absorption, the C-O bond linking CH_3- and -OCO- in CH_3OCO- stretches. And the $CH_3OCOOPF_4$ transforms into TS2, and then it decomposes into CO_2 and CH_3-, releasing energy.

(2) In the second pathway, absorbing heat, the group of $CH_3OCOOPF_4$ breaks at the C-O bind linking POF_4OCO- and CH_3-. And then upon a further heat absorption, the group of POF_4OCO- transforms into TS3 by the P-O bond, which links POF_4 and -OCO- stretching. Then, TS3 decomposes into POF_4 and CO_2, releasing energy.

Figure 4b shows the thermal decomposition reaction pathway of DMC combining with PF_5 in the air environment. And these reactions are consistent with those in the electrolyte environment, except there are some differences in the energy changes during the reaction process. The energy barriers for thermal decomposition for DMC combining with PF_5 reduce significantly compared with those for DMC thermal decomposed independently. And this effect is more pronounced in the electrolyte environment than in the air environment.

3.2.2. Reactions of DMC with POF_3

Figure 5 shows the thermal decomposition reaction pathway of DMC combining with POF_3 in the electrolyte environment and the air environment.

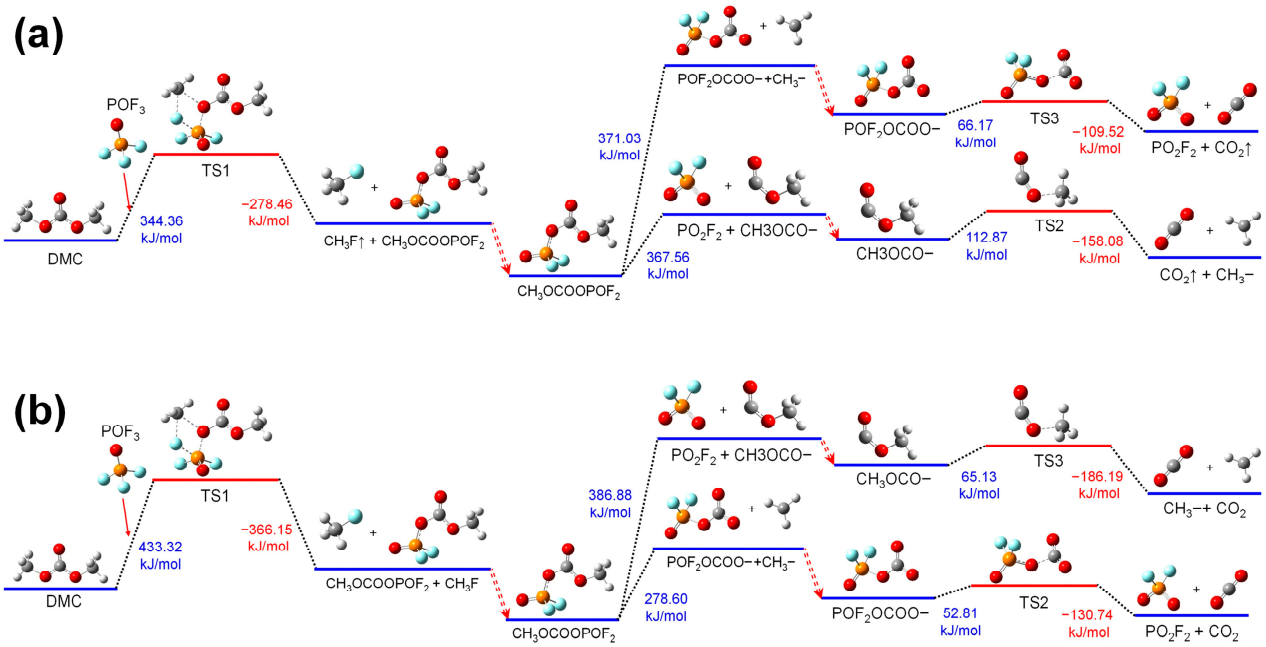

Figure 5. Reaction pathway of DMC with POF_3. Note: (**a**) Reactions in the electrolyte environment; (**b**) reactions in the air environment.

The thermal decomposition reaction mechanisms of DMC combining with POF_3 in both the electrolyte and air environments are analogous to those of DMC combining with PF_5. Given that the oxidizing property of POF_3 is weaker than that of PF_5, the energy absorbed in the ring-opening reactions of DMC combining with POF_3 is higher than that when DMC combines with PF_5.

3.3. Reactions of DEC with PF_5 and POF_3

DEC also plays multiple crucial roles in LIB electrolytes. Similar to DMC, as another linear carbonate solvent, DEC has a low viscosity characteristic, and it significantly enhances the fluidity of the electrolyte. Although DEC and DMC are structurally similar, the differences in their molecular structures result in significant variations in their thermal stability. The essential cause of the difference in their thermal stability lies in the structural effects induced by the groups of CH_3- and C_2H_5-. A longer carbon chain of the C_2H_5- in the DEC molecule endows its more complex reaction characteristics [26].

3.3.1. Reactions of DEC with PF_5

Figure 6a shows the thermal decomposition reaction pathway of DEC combining with PF_5 in the electrolyte environment. The O atom in the ethoxy group of DEC combines with the P atom in PF_5, forming a group of $C_2H_5OCOOC_2H_5$-PF_5. Absorbing heat, the group of $C_2H_5OCOOC_2H_5$-PF_5 undergoes a reaction where one F atom from PF_5 combines with the C_2H_5- from DEC, followed by a further decomposition into C_2H_5F and $C_2H_5OCOOPF_4$. Then the $C_2H_5OCOOPF_4$ undergoes further thermal decomposition reactions divided into two concurrent pathways.

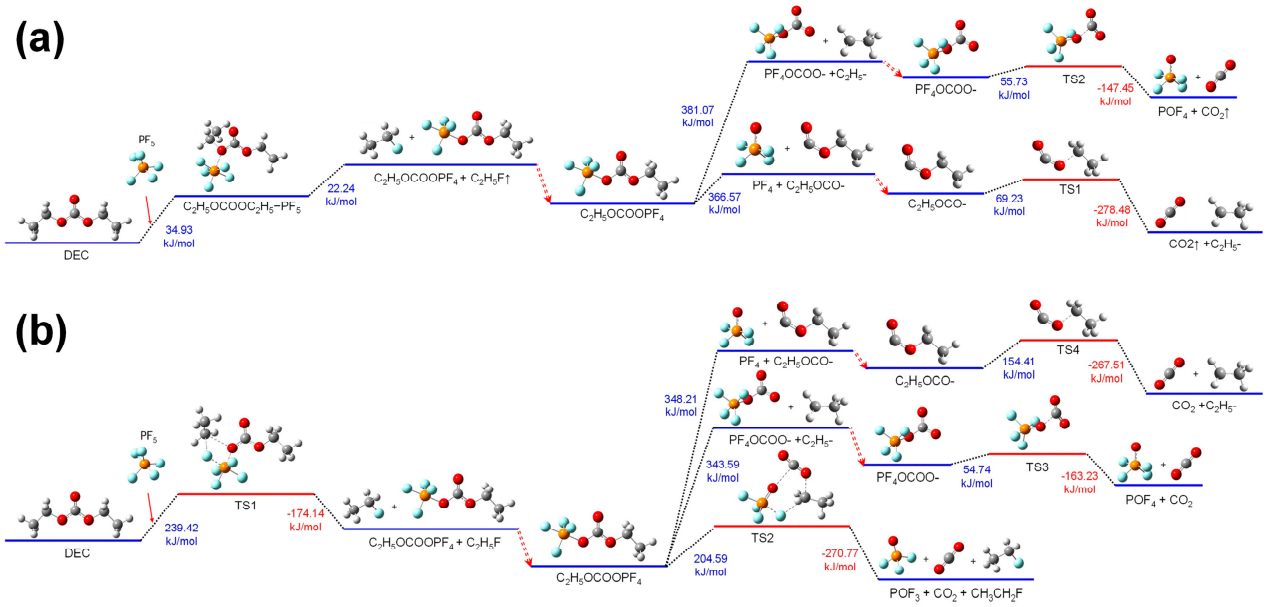

Figure 6. Reaction pathway of DEC with PF_5. Note: (**a**) Reactions in the electrolyte environment; (**b**) reactions in the air environment.

(1) In the first pathway, absorbing heat, the group of $C_2H_5OCOOPF_4$ cleaves at the C-O bond linking PF_4O- and produces groups of POF_4 and C_2H_5OCO-. Then, for the group of C_2H_5OCO-, absorbing heat, the C-O bond linking C_2H_5- and -OCO- stretches to transform into TS1. And the TS1 breaks into C_2H_5- and CO_2, releasing energy.

(2) In the second pathway, absorbing heat, the group of $C_2H_5OCOOPF_4$ cleaves at the C-O bond, on another side, linking C_2H_5-, and produces other groups of C_2H_5- and PF_4OOCO-. Then, for the group of PF_4OOCO-, absorbing heat, the C-O bond linking PF_4O- and -OCO- stretches to transforms into TS2. And the TS2 breaks into POF_4- and CO_2, releasing energy.

Figure 6b shows the thermal decomposition reaction pathway of DEC combining with PF_5 in the air environment. It differs slightly from that in the electrolyte. Absorbing heat, the O atom in the C_2H_5O- group of DEC binds to the P atom in PF_5, while the C atom combines with a F atom in PF_5. Meanwhile, the C-O bond linking C_2H_5- and the P-F bond at the F atom connecting with DEC stretch to transform into a transition state TS1. Then, the TS1 breaks into C_2H_5F and $C_2H_5OCOOPF_4$, releasing energy. $C_2H_5OCOOPF_4$ undergoes further thermal decomposition through three pathways. The first two of these pathways are identical to those in the electrolyte environment, where the $C_2H_5OCOOPF_4$ group undergoes C-O bond cleavage at the C_2H_5- site and the PF_4O site, respectively. However, due to the absence of the solvation effect of the electrolyte environment, their reaction energy has changed.

In the third pathway, absorbing heat, the group of $C_2H_5OCOOPF_4$ undergoes reorganization reactions. The C-O bonds at the C_2H_5- site and PF_4O- site stretch. Simultaneously, a F atom in PF_4O- combines with the C atom of the -CH_2- in C_2H_5-, while the P-F bond at this corresponding F atom stretches. Then, the group of $C_2H_5OCOOPF_4$ transforms into TS2.

The $C_2H_5OCOOPF_4$ group absorbs energy and undergoes reorganization. The C-O bond at the $C_2H_5^-$ site and the C-O bond at the POF_4^- site stretch simultaneously, while the P-F bond in the POF_4^- group stretches. The corresponding fluorine atom combines with the methylene group of the $C_2H_5^-$ group, forming the transition state TS2. Then, TS2 breaks into POF_3, CO_2, and C_2H_5F. This reaction process is similar to the third reaction pathway of the thermal decomposition of EC combining with PF_5 in the air environment.

The reaction mechanisms of thermal decomposition of DEC combined with PF_5 in electrolyte and air environments are similar to those of DMC. DEC is more likely to combine with PF_5 and undergo the first step of thermal decomposition to generate fluorinated hydrocarbons and chain phosphate groups. This is because the bond energy of the C-C bond in the $C_2H_5^-$ group of DEC (approximately 347 kJ/mol) is lower than that of the C-H bond in the CH_3^- group of DMC (approximately 413 kJ/mol). At high temperatures, the C-C bond in DEC is more prone to cleavage, leading to molecular decomposition [36]. During the further thermal decomposition process of the chain phosphate groups of $C_2H_5OCOOPF_4$, the hyperconjugation effect of $C_2H_5^-$ in $C_2H_5OCOOPF_4$ enhances its local thermal stability, resulting in slightly higher energy consumption for some of its subsequent thermal decomposition reactions compared with $CH_3OCOOPF_4$ produced by DMC's reactions with PF_5.

3.3.2. Reactions of DEC with POF_3

Figure 7 shows the thermal decomposition reaction pathway of DEC combining with POF_3 in the electrolyte environment and the air environment.

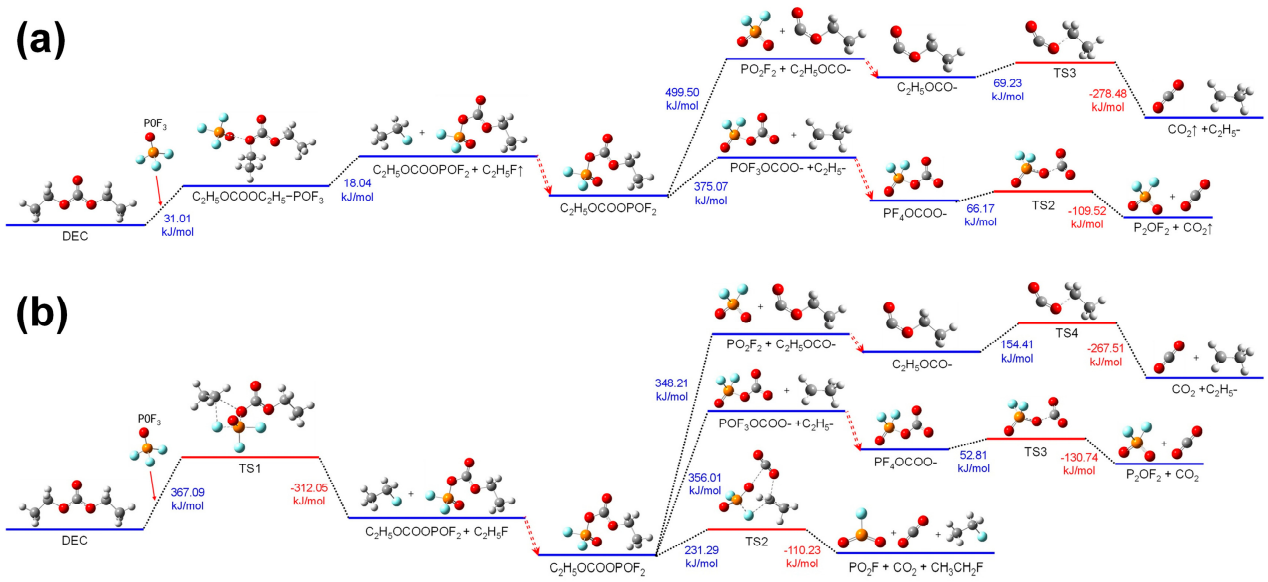

Figure 7. Reaction pathway of DEC with POF_3. Note: (**a**) Reactions in the electrolyte environment; (**b**) reactions in the air environment.

The thermal decomposition reaction mechanisms of DEC combining with POF_3 in both electrolyte and air environments are analogous to those of DEC combining with POF_3. Compared with DMC, DEC is more prone to undergoing thermal decomposition after combining with POF_3. This is attributed to the stronger electron-donating property of the C_2H_5- in DEC, which enables DEC to more easily combine with POF_3 in a solution environment and undergo further decomposition reactions.

In summary, both PF_5 and POF_3 can promote the thermal decomposition reactions of EC, DMC, and DEC, whether in the electrolyte environment or the air environment. The chain structure of DMC and DEC makes them more prone to combining with PF_5 and POF_3. DEC is more prone to combining with PF_5 and POF_3 and undergoing thermal decomposition reactions than DMC. Compared with DMC, after combining with PF_5 or POF_3, EC and DEC could undergo recombination reactions with lower energy consumption. Therefore, PF_5 and POF_3 exhibit a more significant promoting effect on their thermal decomposition of EC and DEC. And this regularity is consistent with the results of experimental studies on the thermal analysis of electrolytes [20,24].

The reaction mechanism model for the thermal decomposition of the electrolyte catalyzed by PF_5 and POF_3 proposed by this research group has promoted a leap in the field of lithium-ion battery thermal runaway research from phenomenological observation to mechanism-based regulation. PF_5 and POF_3 activate the ester groups of carbonate molecules in the electrolyte through a Lewis acid catalytic mechanism, which reduces the activation energy for C-O bond cleavage, accelerates the formation of low-carbon chain aldehyde and ketone products, and further triggers fluorination reactions, ultimately leading to the formation of an acid catalysis chain propagation vicious cycle. This insight fills the theoretical gap regarding how lithium salt decomposition products quantitatively affect the thermal stability of electrolytes and corrects the previous one-sided research perspective of only focusing on the thermal stability of the lithium salts themselves. Based on the understanding of the active sites and catalytic pathways of PF_5 and POF_3 in the reaction model, we can develop electrolyte additives by targeting the Lewis acid activity of PF_5, which can block the catalytic reaction sites through coordination. This mechanism-guided research and developed model replaces the traditional trial-and-error method and significantly improves the efficiency of electrolyte modification. Meanwhile, the intermediate products from the reactions of PF_5 and POF_3 with the electrolyte can serve as molecular-level indicators for thermal runaway early warning and protection. This provides a theoretical basis for the development of high sensitivity gas sensors and the construction of multi-level early warning systems, thereby enabling the early identification and intervention of thermal runaway risks.

3.4. The Inhibitory Effects of Fluorinated Electrolytes on the Promotions of PF_5 and POF_3

Compared with EC, DMC, and DEC, fluorinated carbonate electrolytes exhibit better thermal stability. The strong electron-withdrawing effect of F atoms in fluorinated carbonate electrolytes enhances the antioxidant capacity of the electrolytes and significantly strengthens the promoting effect on the thermal decomposition reactions of PF_5 and POF_3. In this part, we analyze the energy consumption of the fluorinated electrolytes, FEC, FDMC, and FDEC, during their combination with PF_5 and POF_3. The molecular models of FEC, FDMC, and FDEC are shown in Figure S3.

3.4.1. Inhibitory Effects of FEC for Thermal Decomposition

The energy consumption during the reactions of EC and FEC with PF_5 and POF_3 are shown in Table 2 and Figure S4a.

Compared with the EC molecule, in the FEC molecule, one H atom on the -CH_2- group in its cyclic structure is replaced by a F atom. The FEC molecule presents an asymmetric structure different from a centrally symmetric structure of an EC molecule. Therefore, there are two different combining modes between FEC and PF_5 as well as POF_3. The first reaction mode is the same as that of EC. PF_5 or POF_3 molecules combine with the -CH_2- and -O- on the side of FEC that does not contain F atoms, followed by a ring-opening reaction. And the other reaction mode is that PF_5 or POF_3 molecules combine with the -CHF- and -O- on the F-containing side of FEC, followed by a ring-opening reaction. Compared with EC, whether in the electrolyte or the air environment, the energy consumption during FEC combining with PF_5 or POF_3 increases. Therefore, the antioxidant capacity of FEC during the thermal runaway process is significantly better than that of EC.

Table 2. Energy consumption for EC or FEC combining with PF_5 or POF_3.

No.	Constituents	Reaction	Environment	E/(kJ/mol)	Ration
1	EC	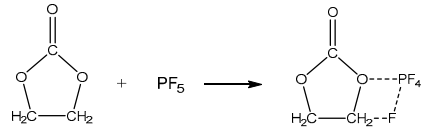	Electrolyte	185.37	-
2			Air	275.39	-
3		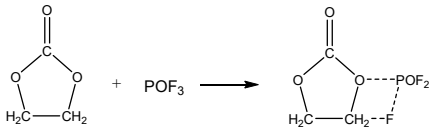	Electrolyte	303.07	-
4			Air	409.05	-
5	FEC	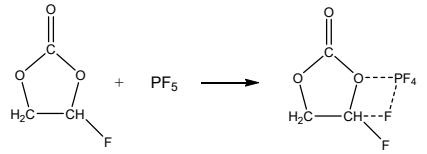	Electrolyte	264.71	42.80%
6			Air	329.31	77.65%
7		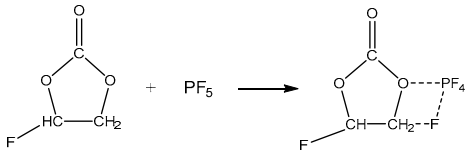	Electrolyte	194.32	4.83%
8			Air	279.53	1.50%
9		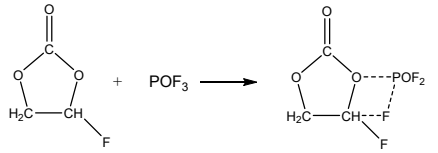	Electrolyte	339.17	11.91%
10			Air	409.07	0.00%
11		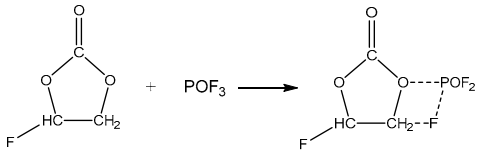	Electrolyte	404.97	33.62%
12			Air	470.49	15.02%

Note: Ration = $(E_{FEC} - E_{EC})/E_{EC} \times 100\%$.

3.4.2. Inhibitory Effects of FDMC for Thermal Decomposition

The energy consumption during the reactions of DMC and FDMC with PF_5 and POF_3 are shown in Table 3 and Figure S4b.

Table 3. Energy consumption for DMC or FDMC combining with PF_5 or POF_3.

No.	Constituents	Reaction	Environment	E/(kJ/mol)	Ration
1	DMC	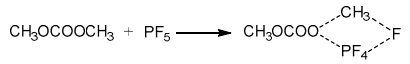	Electrolyte	22.72	-
2			Air	294.96	-
3		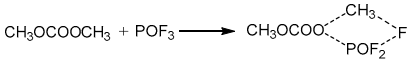	Electrolyte	344.36	-
4			Air	433.32	-
5	FDMC		Electrolyte	189.41	733.67%
6			Air	606.83	105.73%
7			Electrolyte	469.45	36.33%
8			Air	755.95	74.46%

Note: Ration = $(E_{FEC} - E_{EC})/E_{EC} \times 100\%$.

Compared with the DMC molecule, in the FDMC molecule, one H atom on the terminal CH_3- group of its chain structure is replaced by a F atom. FDMC also has two combining modes with PF_5 or POF_3. In the first mode, the reaction process and energy consumption of PF_5 or POF_3 combining with the C atom and O atom on the -CH_3 side in FDMC are almost the same as those in DMC. And in the second mode, PF_5 or POF_3 combines with the C atom and O atom on the FCH_2- side in FDMC. Compared with DMC,

in the electrolyte environment, the energy consumed by the combination of FDMC with PF_5 and POF_3 increases by 733.67% and 36.33%, respectively; in the air environment, the energy consumed by the combination of FDMC with PF_5 and POF_3 rises by 105.73% and 74.46%, respectively. So, the antioxidant capacity of FDMC during the thermal runaway process is significantly superior to that of DMC.

3.4.3. Inhibitory Effects of FDEC for Thermal Decomposition

The energy consumption during the reactions of DEC and FDEC with PF_5 and POF_3 are shown in Table 4 and Figure S4c.

Table 4. Energy consumption for DEC or FDEC combining with PF_5 or POF_3.

No.	Constituents	Reaction	Environment	E/(kJ/mol)	Ration
1	DEC	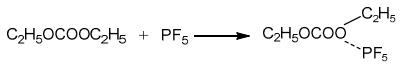	Electrolyte	34.93	-
2		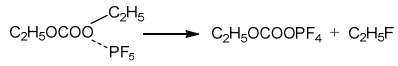		22.24	-
3		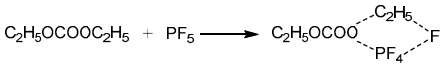	Air	239.42	-
4		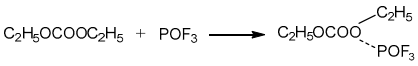	Electrolyte	31.01	-
5		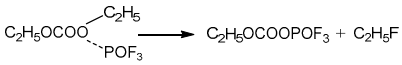		18.04	-
6		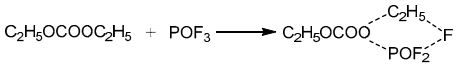	Air	367.09	-
7	FDEC	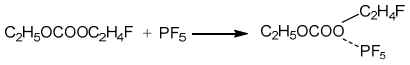	Electrolyte	28.98	−96.17%
8		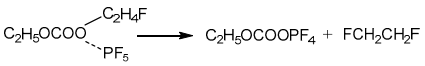		234.64	571.74%
9		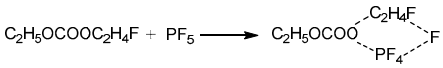	Air	254.57	6.33%
10		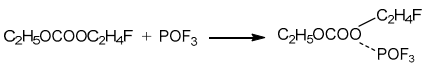	Electrolyte	31.11	−87.01%
11		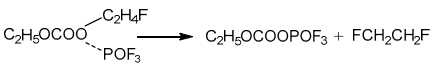		226.75	631.22%
12		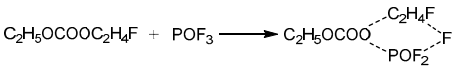	Air	389.48	6.10%

Note: Ration = $(E_{FEC} - E_{EC})/E_{EC} \times 100\%$.

Compared with DMC, DEC has more fluorinated substitution sites. In this part, the reactivity of the FDEC molecule ($C_2H_5OCOOCH_2CH_2F$), where the H atom at the terminal CH_3- position of DEC is replaced by a F atom, is analyzed.

In the electrolyte environment, both of the DEC and FDEC molecules first combine with PF_5 or POF_3 and then continue to undergo thermal decomposition reactions. Compared with DEC, the energy consumed during the binding process of FDEC with PF_5 or POF_3 decreases slightly, but the energy consumed in the subsequent thermal decomposition reactions increases by 212.40 kJ/mol and 208.71 kJ/mol, respectively (rising by 571.74% and 631.22%, respectively). Therefore, the antioxidant capacity of FDEC during the thermal runaway process is significantly improved compared with that of DEC. In the air environment, both DEC and FDEC combine with PF_5 or POF_3 and absorb heat, transforming into transition state substances. The energies absorbed during these processes and their further thermal decomposition reactions increase by 6.33% and 6.10%, respectively.

In summary, fluorinated electrolytes can significantly increase the energy required for their binding process with PF_5 and POF_3, inhibiting the promoting effect on their thermal decomposition during thermal runaway of LIBs. Therefore, in the design of LIB systems and the preparation of electrolytes, the usage of fluorinated electrolytes can significantly improve LIBs' thermal stability and enhance their safety performance.

In LIBs, the conventional lithium salt $LiPF_6$ is recognized as one of the critical factors contributing to the risk of electrolyte thermal runaway. When the battery temperature rises, $LiPF_6$ tends to decompose readily, generating reactive species such as PF_5 and POF_3. These two substances further catalyze the thermal decomposition of the electrolyte, forming a vicious cycle of catalysis-accelerated decomposition and exacerbating the potential hazard of battery thermal runaway.

If $LiPF_6$ is replaced with more stable lithium salts such as LiFSI, LiBF, or LiTFSI, the formation of PF_5 and POF_3 can be eliminated at the source. Such alternative lithium salts do not contain labile P-F bonds in their molecular structures, so they are less prone to decomposing and producing reactive catalytic substances under high-temperature conditions, fundamentally breaking the chain of reactive species generation-catalyzed electrolyte decomposition.

Meanwhile, alternative lithium salts can also optimize the interfacial stability of the electrolyte, reduce the side reactions between the electrolyte and electrodes at high temperatures, and further decrease the heat generation rate. This dual effect not only inhibits the thermal decomposition process of the electrolyte but also significantly enhances the overall thermal stability of LIBs. It provides crucial support for the safe operation of LIBs in high-temperature environments and holds great significance for the safety performance upgrading in fields such as new energy vehicles and energy storage systems.

4. Conclusions

In this paper, quantum chemical calculation methods are employed to investigate the reaction processes between PF_5 and POF_3 and EC, DMC, and DEC during the thermal runaway of LIBs, under both electrolyte and air environments. Furthermore, a comprehensive chemical reaction mechanism model is constructed. The main research findings of this paper are as follows:

(1) During the thermal runaway process of LIBs, PF_5 and POF_3 generated by the thermal decomposition of $LiPF_6$ can significantly promote the thermal decomposition of the electrolytes. The P atoms in PF_5 or POF_3 combine with the O atoms of the ether oxygen groups in carbonates, while the F atoms combine with the C atoms adjacent to the ether oxygen groups, promoting the ring-opening or chain scission of the carbonate molecules. When EC, DMC, and DEC combine with PF_5 or POF_3, the energies required for their thermal decomposition reactions decrease, which promotes the combustion of the electrolyte and the generation of fire gases.

(2) Fluorination can effectively inhibit the promoting effect of PF_5 and POF_3 on the thermal decomposition reaction of the electrolyte. Fluorinated modification of the alkyl groups in EC, DMC, and DEC molecules can form FEC, FDMC, and FDEC. And the consumed energies of the thermal decomposition of FEC, FDMC, and FDEC combining to PF_5 or POF_3 are significantly increased, which can effectively enhance the antioxidant property of the electrolyte.

It should be specifically noted that the thermal decomposition reactions during the thermal runaway of LIBs are highly complex, which result from the interaction and accumulation of multiple chemical reactions. The quantum chemical calculations in this study can provide a theoretical basis for understanding the complex reactions in the thermal runaway process.

Supplementary Materials: The following supporting information can be downloaded at https://www.mdpi.com/article/10.3390/fire8090370/s1, Figure S1(a): Thermal decomposition reaction pathways of $LiPF_6$ with H_2O in the electrolyte; Figure S1(b): Thermal decomposition reaction pathways of $LiPF_6$ with EC in the electrolyte; Figure S1(c): Thermal decomposition reaction pathways of $LiPF_6$ with DMC in the electrolyte; Figure S2: HOMO and LUMO energy levels of key productions during thermal decomposition of LiPF6 in the electrolyte and air environment; Figure S3: Configurations of fluorinated electrolytes; Figure S4(a): Energy Consumption for FEC Combining with PF_5 or POF_3; Figure S4(b): Energy Consumption for FDMC Combining with PF_5 or POF_3; Figure S4(c): Energy Consumption for FDEC Combining with PF_5 or POF_3.

Author Contributions: Conceptualization, Y.T. and Z.C.; methodology, X.Z. (Xiaotiao Zhan), Z.Q., Q.X. and X.Z. (Xia Zhang); software, Y.T. and Y.L.; validation, X.Z. (Xia Zhang), Z.C. and Y.T.; formal analysis, Y.T., X.Z. (Xiaotiao Zhan), Y.Z., Y.L., J.L. and Z.C.; investigation, Y.Z., Z.Q., and Q.X.; resources, J.L., X.Z. (Xia Zhang) and Z.C.; data curation, Y.Z., Y.L. and X.Z. (Xia Zhang); writing—original draft preparation, Y.T., X.Z. (Xiaotiao Zhan), X.Z. (Xia Zhang). and Z.C.; writing—review and editing, Y.T., J.L. and Z.C.; visualization, Y.T., Q.X., X.Z. (Xia Zhang) and Z.C.; supervision, Y.T. and Z.C.; project administration, Y.T. and Z.C.; funding acquisition, Y.T., J.L., Q.X., X.Z. (Xia Zhang) and Z.C. All authors have read and agreed to the published version of the manuscript.

Funding: The authors declare that financial support was received for the research, authorship, and/or publication of this article. This research was financially supported by the Shenzhen Science and Technology Program (KCXFZ20211020163810015), Shenzhen Science and Technology Program (KCXST20221021111201003), National Natural Science Foundation of China (No. 52261160384, 52072208 and C0072140), Fundamental Research Project of Shenzhen (No. JCYJ20220818101004009), Local Innovative and Research Teams Project of Guangdong Pearl River Talents Program (2017BT01N111), Guangdong Basic and Applied Basic Research Foundation (No. 2022A1515110531), China Postdoctoral Science Foundation (No. 2022M721800), Shenzhen Engineering Research Center on Key Technology of Next-Generation Power and Energy-Storage Battery (XMHT20230108012), University Research & Development Project of Shenzhen Polytechnic University (no. 513-602431Y003P), and Key-Area Research and Development Program of Guangdong Province (2023B0909030001).

Data Availability Statement: The original contributions presented in the study are included in the article/Supplementary Materials; further inquiries can be directed to the corresponding authors.

Acknowledgments: We also acknowledge the support of the Testing Technology Center of Materials and Devices of Tsinghua Shenzhen International Graduate School (SIGS); and the Major Science and Technology Infrastructure Project of the Material Genome Big-science Facilities Platform, supported by the Municipal Development and Reform Commission of Shenzhen.

Conflicts of Interest: The authors declare that the research was conducted in the absence of any commercial or financial relationships that could be construed as potential conflicts of interest.

References

1. EVTank. *China Lithium-Ion Battery Industry Development White Paper (2025)*; China YiWei Institute of Economics: Beijing, China, 2025.
2. Wang, Q.; Huang, P.; Ping, P.; Du, Y.; Li, K.; Sun, J. Combustion behavior of lithium iron phosphate battery induced by external heat radiation. *J. Loss Prev. Process Ind.* **2017**, *49*, 961–969. [CrossRef]
3. Wang, Q.; Jiang, L.; Yu, Y.; Sun, J. Progress of enhancing the safety of lithium ion battery from the electrolyte aspect. *Nano Energy* **2019**, *55*, 93–114. [CrossRef]
4. Feng, X.; Fang, M.; He, X.; Ouyang, M.; Lu, L.; Wang, H.; Zhang, M. Thermal runaway features of large format prismatic lithium ion battery using extended volume accelerating rate calorimetry. *J. Power Sources* **2014**, *255*, 294–301. [CrossRef]
5. Feng, X.; Ouyang, M.; Liu, X.; Lu, L.; Xia, Y.; He, X. Thermal runaway mechanism of lithium ion battery for electric vehicles: A review. *Energy Storage Mater.* **2018**, *10*, 246–267. [CrossRef]
6. Golubkov, A.W.; Fuchs, D.; Wagner, J.; Wiltsche, H.; Stangl, C.; Fauler, G.; Voitic, G.; Thaler, A.; Hacker, V. Thermal-runaway experiments on consumer Li-ion batteries with metal-oxide and olivin-type cathodes. *RSC Adv.* **2014**, *4*, 3633–3642. [CrossRef]

7. Sun, J.; Li, J.; Zhou, T.; Yang, K.; Wei, S.; Tang, N.; Dang, N.; Li, H.; Qiu, X.; Chen, L. Toxicity, a serious concern of thermal runaway from commercial Li-ion battery. *Nano Energy* **2016**, *27*, 313–319. [CrossRef]
8. Sun, P.; Bisschop, R.; Niu, H.; Huang, X. Correction to: A Review of Battery Fires in Electric Vehicles. *Fire Technol.* **2020**, *56*, 1411. [CrossRef]
9. Wang, Q.; Sun, J.; Yao, X.; Chen, C. C80 Calorimeter Studies of the Thermal Behavior of LiPF6 Solutions. *J. Solut. Chem.* **2006**, *35*, 179–189. [CrossRef]
10. Tokihiko, Y.; Daikichi, M.; Fujio, M.; Tetsuya, O.; Koji, T.; Shun, E.; Satomi, N.; Satoru, I.; Koichi, Y. Direct observation of internal state of thermal runaway in lithium ion battery during nail-penetration test. *J. Power Sources* **2018**, *393*, 67–74. [CrossRef]
11. Chen, Y.; Kang, Y.; Zhao, Y.; Wang, L.; Liu, J.; Li, Y.; Liang, Z.; He, X.; Li, X.; Tavajoh, N.; et al. A review of lithium-ion battery safety concerns: The issues, strategies, and testing standards. *J. Energy Chem.* **2021**, *59*, 83–99. [CrossRef]
12. Ouyang, D.; Weng, J.; Chen, M.; Liu, J.; Wang, J. Experimental analysis on the degradation behavior of overdischarged lithium-ion. *Energy Res.* **2020**, *44*, 229–241. [CrossRef]
13. Wahyudi, W.; Guo, X.; Ladelta, V.; Tsetseris, L.; Nugraha, M.; Lin, N.; Tung, V.; Hadjichristidis, N.; Li, Q.; Xu, K.; et al. Hitherto Unknown Solvent and Anion Pairs in Solvation Structures Reveal New Insights into High-Performance Lithium-Ion Batteries. *Adv. Sci.* **2022**, *28*, 2202405. [CrossRef]
14. Hui, Y.; Guorong, V.Z.; Philip, N.R. Thermal Stability of LiPF6 Salt and Li-ion Battery Electrolytes Containing LiPF6. *J. Power Sources* **2006**, *161*, 573–579.
15. Christopher, L.C.; Wentao, L.; Brett, L.L. Thermal Decomposition of LiPF6-Based Electrolytes for Lithium-Ion Batteries. *J. Electrochem. Soc.* **2005**, *152*, A2327–A2334.
16. Gnanaraja, J.S.; Zinigrada, E.; Asrafa, L.; Gottlieb, H.; Sprecher, M.; Aurbach, D.; Schmidt, M. The use of accelerating rate calorimetry (ARC) for the study of the thermal reactions of Li-ion battery electrolyte solutions. *J. Power Sources* **2003**, *119–121*, 794–798. [CrossRef]
17. Tasaki, K.; Kanda, K.; Nakamura, S.; Ue, M. Decomposition of LiPF6 and Stability of PF5 in Li-Ion Battery Electrolytes Density Functional Theory and Molecular Dynamics Studies. *J. Electrochem. Soc.* **2003**, *150*, A1628–A1636. [CrossRef]
18. Spotte-Smith, E.W.C.; Thea, B.P.; Hetal, D.P.; Samuel, M.B.; Kristin, A.P. Elementary Decomposition Mechanisms of Lithium Hexafluorophosphate in Battery Electrolytes and Interphases. *ACS Energy Lett.* **2023**, *8*, 347–355. [CrossRef]
19. Wang, Q.; Sun, J.; Chu, G.; Yao, X.; Chen, C. Effect of LiPF6 on the thermal behaviors of four organic solvents for lithium ion batteries. *J. Therm. Anal. Calorim.* **2007**, *89*, 245–250. [CrossRef]
20. Miyoshi, S.; Nagano, H.; Fukuda, T.; Kurihara, T.; Watanabe, M.; Ida, S.; Ishihara, T. Dual-Carbon Battery Using High Concentration LiPF6 in Dimethyl Carbonate (DMC) Electrolyte. *J. Electrochem. Soc.* **2016**, *163*, A1206–A1213. [CrossRef]
21. Tian, Y.; Zhao, Y.; Kang, Y.; Wu, J.; Meng, Y.; Hu, X.; Huang, M.; Lan, B.; Kang, F.; Li, B. Quantum chemical calculation study on the thermal decomposition of electrolyte during lithium-ion battery thermal runaway. *Front. Energy Res.* **2024**, *12*, 120497. [CrossRef]
22. Ella, Z.; Liraz, L.; Josef, S.G.; Milon, S.; Doron, A. On the thermal stability of LiPF6. *Thermochim. Acta* **2005**, *438*, 184–191. [CrossRef]
23. Sloop, S.E.; Pugh, J.K.; Wang, S.; Kerr, J.B.; Kinoshita, K. Chemical Reactivity of PF5 and LiPF6 in Ethylene Carbonate/Dimethyl Carbonate Solutions. *Electrochem. Solid-State Lett.* **2001**, *4*, A42–A44. [CrossRef]
24. Bernardine, L.D.R.; David, S.H.; Israel, T.; Clare, P.G. Electrolyte Oxidation Pathways in Lithium-Ion Batteries. *J. Am. Chem. Soc.* **2020**, *142*, 15058–15074.
25. Tetsuya, K.; Arihisa, K.; Minato, E.; Shigeto, O.; Jun-Ichi, Y. Thermal stability of alkyl carbonate mixed-solvent electrolytes for lithium ion cells. *J. Power Sources* **2002**, *104*, 260–264. [CrossRef]
26. Lamb, J.; Orendorff, C.J.; Roth, E.P.; Langendorf, J. Studies on the Thermal Breakdown of Common Li-Ion Battery Electrolyte Components. *J. Electrochem. Soc.* **2015**, *162*, A2131–A2135. [CrossRef]
27. Gerardine, G.B.; Ralph, E.W.; Zhang, Z. Thermal stability of $LiPF_6$-EC:EMC electrolyte for lithium ion batteries. *J. Power Sources* **2001**, *97–98*, 570–575.
28. Jia, Z.; Wang, S.; Qin, P.; Li, C.; Jin, K.; Sun, J.; Wang, Q. Investigation of gas diffusion behavior and detection of 86 Ah LiFePO4 batteries in energy storage systems during thermal runaway. *Process Saf. Environ. Prot.* **2024**, *184*, 579–588. [CrossRef]
29. Xie, J.; Li, J.; Wang, J.; Jiang, J. Fire protection design of a lithium-ion battery warehouse based on numerical simulation results. *J. Loss Prev. Process Ind.* **2022**, *80*, 104885. [CrossRef]
30. Barré, P.; Guibaud, A. Numerical investigation of the influence of thermal runaway modelling on car park fire hazard and application to a Lithium-ion Manganese Oxide battery. *Fire Saf. J.* **2024**, *150*, 104284. [CrossRef]
31. Okamoto, Y. Ab Initio Calculations of Thermal Decomposition Mechanism of LiPF6-Based Electrolytes for Lithium-Ion Batteries. *J. Electrochem. Soc.* **2013**, *160*, A404–A409. [CrossRef]
32. Tian, Y.; Zhang, X.; Xia, Q.; Chen, Z. Oxidation Mechanisms of Electrolyte and Fire Gas Generation Laws During a Lithium-Ion Battery Thermal Runaway. *Fire* **2025**, *8*, 226. [CrossRef]

33. Frisch, J.M.; Trucks, G.W.; Schlegel, H.B.; Scuseria, G.E.; Robb, M.A.; Cheeseman, J.R.; Scalmani, G.; Barone, V.; Petersson, G.A.; Nakatsuji, H.; et al. *Gaussian 16*; Revision C.01; Gaussian, Inc.: Wallingford, CT, USA, 2016.
34. Dennington, R.; Keith, T.A.; Millam, J.M. *GaussView*; Version 6.0; Semichem Inc.: Shawnee Mission, KS, USA, 2016.
35. Chen, X.; Zhang, X.; Li, H.; Zhang, Q. Cation-solvent, cation-anion, and solvent-solvent interactions with electrolyte solvation in lithium batteries. *Batter. Supercaps* **2019**, *2*, 128–131. [CrossRef]
36. Sun, W.; Huang, C.; Tao, T.; Zhang, F.; Li, W.; Hansen, N.; Yang, B. Exploring the high-temperature kinetics of diethyl carbonate (DEC) under pyrolysis and flame conditions. *Combust. Flame* **2017**, *181*, 71–81. [CrossRef]

Disclaimer/Publisher's Note: The statements, opinions and data contained in all publications are solely those of the individual author(s) and contributor(s) and not of MDPI and/or the editor(s). MDPI and/or the editor(s) disclaim responsibility for any injury to people or property resulting from any ideas, methods, instructions or products referred to in the content.